Int. J. Heat Mass Transfer. Vol. 25, No. 9, pp. 1301–1312, 1982
Printed in Great Britain

0017–9310/82/091301–12 $03.00/0
Pergamon Press Ltd.

FLOODING IN VERTICAL GAS–LIQUID COUNTERCURRENT FLOW THROUGH MULTIPLE SHORT PATHS

C. P. LIU*, G. E. MCCARTHY and C. L. TIEN
Department of Mechanical Engineering, University of California, Berkeley, CA 94720, U.S.A.

(*Received* 29 *March* 1982)

Abstract—An experimental investigation has been conducted on flooding in the vertical gas–liquid countercurrent flow through multiple short paths. Experimental results show similar flooding characteristics as those in the single-path flow, but secondary behaviors also exist, unique to the multiple-path flow, due to path interaction. A modeling procedure has been developed to analyze the onset of flooding. The analysis shows that correlations of the Wallis and Kutateladze type may be interpreted as dynamic similarity conditions for the flooding phenomenon, although their detailed parametric dependences are quite complicated.

NOMENCLATURE

A_i, gas flow area blockage [m^2];
C_i, proportionality constant;
c_K, experimental constant defined in equation (4);
c_W, experimental constant defined in equation (1);
D, path diameter [m];
g, gravitational constant [$m\,s^{-2}$];
H, maximum height attained by the gas–liquid mixture [m];
j_i, superficial velocity [$m\,s^{-1}$];
m, experimental constant defined in equation (1);
ΔM_i, change in momentum [N];
Δp, change in gas pressure [$N\,m^{-2}$];
Δp_n, change in gas pressure in each individual path [$N\,m^{-2}$];
Q_i, volumetric flow rate [$m^3\,s^{-1}$];
Q_{in}, volumetric flow rate in each individual path [$m^3\,s^{-1}$];
R, path radius [m];
U_i, average velocity based on the actual flow area [$m\,s^{-1}$].

Greek symbols

δ, film thickness [m];
λ, characteristic length [m];
μ, viscosity [$k\,m^{-1}\,s^{-1}$];
ρ_i, density [$kg\,m^{-3}$];
σ, surface tension [$N\,m^{-1}$].

Subscripts

g, gas;
l, liquid.

Dimensionless groups

Im, dimensionless constant defined in equation (23);
J_i, dimensionless superficial velocity defined in equation (2);
K_i, Kutateladze variable defined in equation (5);
K_i', dimensionless superficial velocity defined in equation (23).

INTRODUCTION

GAS–LIQUID countercurrent flow is used extensively in industry for heat and mass transfer purposes. Usually the two fluids are brought into contact inside a vertical pipe or channel where the liquid feeds under gravity. The counterflowing streams usually assume one of two basic configurations: separated flow or active mixing. The separated-flow configuration refers to the situation where each of the two flows (gas and liquid) forms a continuous stream, whereas the active mixing refers to an extensive interaction between the two phases marked by the appearance of liquid agitation. For a given liquid injection rate, there is a critical gas injection rate above which the two flows will mix vigorously and vice versa.

In this paper, the attention is on the onset of flooding, where flooding means the building up of gas–liquid mixture inside a flow system. The onset of flooding thus refers to the first instance when the mixture starts to build up, as a result of change of flow configuration from separated to mixing flow. This onset point marks the transition from a weak gas–liquid interaction (separated flow) to a strong one (mixing). The flooding point and the countercurrent flow limit (CCFL) referred to in the existing literature usually require the mixture to fill up the entire flow path. In this respect, the onset of flooding here may be considered as the flooding point (or CCFL) with very little mixture buildup inside the path.

EXISTING CORRELATIONS

There has been a substantial amount of work done on countercurrent flooding. Tien and Liu have surveyed the flooding studies in both single channels [1] and multiple-paths [2]. A brief review of the various research highlights is given below.

* Present address: Sohio Petroleum Company, Reservoir Engineering Department, San Francisco, CA 94111, U.S.A.

Based on the numerous experimental studies on single-channel flow, the most commonly accepted flooding correlation has been the Wallis correlation [3]

$$J_g^{1/2} + m J_l^{1/2} = c_W \tag{1}$$

where $m \approx 1.0$, and $c_W \approx 0.7$–1.0, depending on the channel inlet geometries. The dimensionless volumetric fluxes for gas and liquid are defined by

$$J_i = \frac{\rho_i^{1/2} j_i}{[g\lambda(\rho_l - \rho_g)]^{1/2}} \quad (i = g, l) \tag{2}$$

where j_i is the superficial velocity, ρ the density, and g the gravitational constant. The characteristic length λ is commonly taken as the hydraulic diameter or the radius of curvature of the flow path.

Tien [4] proposed a similar correlation, taking interfacial instability into consideration by replacing λ with a natural characteristic wavelength of interfacial wave

$$\lambda = \left[\frac{\sigma}{g(\rho_l - \rho_g)}\right]^{1/2} \tag{3}$$

where σ denotes surface tension. Equation (1) can be alternatively expressed as

$$K_g^{1/2} + mK_l^{1/2} = c_K \tag{4}$$

where $c_K \approx 1.7$ 2.0, depending on channel inlet geometries, and

$$K_i = \frac{\rho_i^{1/2} j_i}{[g\sigma(\rho_l - \rho_g)]^{1/4}} \quad (i = l, g). \tag{5}$$

The parameter K_g, commonly called the Kutateladze number, was first established through dimensional analysis of interfacial instability by Kutateladze [5]. The above correlation, known as the Kutateladze correlation, has been increasingly used for correlating flooding data in recent years [1].

A considerable amount of analytical work has been done on predicting the critical flow rates for the onset of flooding in single-channel countercurrent flow. Existing analytical models focus mainly on the annular flow conditions inside the channel, treating the flow either as a hanging film or as a falling film with counterflowing gas stream [1]. Analyses based on the concept of small disturbance appear to have a limited success in elucidating some of the basic single-channel flooding mechanisms.

The majority of existing work on countercurrent flow through multiple short paths are in chemical engineering literature dealing with operations of distillation and absorption columns, and are largely experimental in nature [2]. Analytical efforts have been scarce, and the existing works deal mostly with the bulk behavior of the froth layer (gas–liquid mixture on the plate) rather than the local flow behavior through the perforations. In general, these analyses are at best semi-empirical.

EXPERIMENTAL APPARATUS AND PROCEDURE

A schematic diagram of the experimental system is shown in Fig. 1. The system was made up of two subsystems: the fluid circulation and the instrumentation system. The fluid circulation system consisted of an upper and a lower plenum, a test section, a liquid recirculation loop, and an air injection unit. The instrumentation was made up of venturi meters for both air and liquid flow measurement; a separate collection cylinder was provided for average liquid draining rate measurement. Pressure readings from the venturis were recorded by strip-chart recorders via pressure transducers. A detailed description of the experimental system is given elsewhere [6].

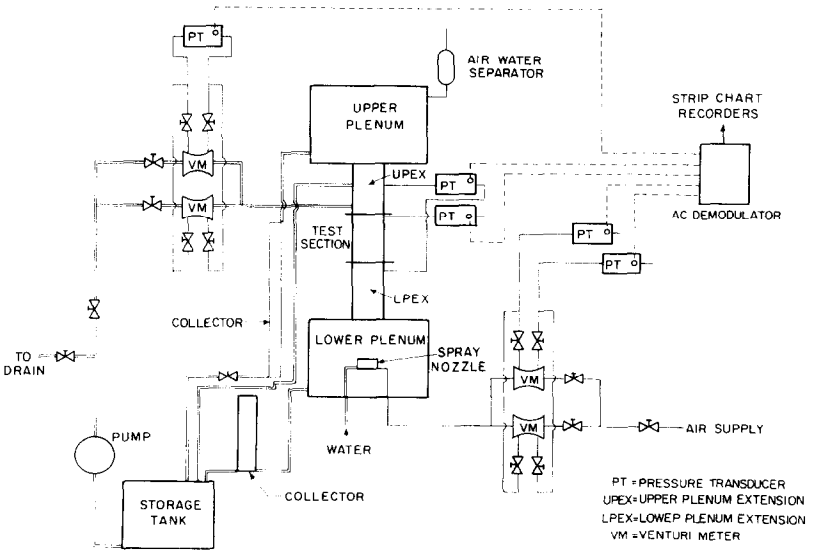

FIG. 1. Experimental system schematic.

The experimental procedure was as follows. The flow paths were first purged by injecting air in rapid pulses to ensure uniform initial conditions. This injection served to create a dry path-wall surface and to remove the excess water build-up around the path inlet. Then the water injection was set at a given level and allowed to reach a steady state; approximately 0.5 min was alloted for this purpose. Since the water flow rate was monitored with a strip chart recorder, the steadiness of the flow was easily verified. After steady water flow had been established, air flow was gradually increased until the criterion for the onset of flooding was met. The criterion corresponded to an agitated appearance of the water pool above the test section. Once the system was induced to flood, both the air and the water flow were shut off, and the same procedure was repeated for the next water flow rate setting.

Because of the large number of test sections used in this experiment, it is much more convenient to refer to a particular test section by its designation. The designation system used here was designed to include all the relevant dimensions of the test section; for example, in a particular test section designation TS-0.5-0.5-7-1.25, the letter T simply stands for test, the letter S is for stub entry (for plate entry, S is replaced with P), the first set of digits is the path diameter in in. (0.5 in), the second set is the path length in in. (0.5 in), the third set is the number of paths (7), and the last set gives the path spacing in in. (1.25 in). A typical test section geometry is shown in Fig. 2.

RESULTS AND DISCUSSION

For countercurrent flow through multiple short paths, the onset of flooding was always preceded by the bending (or lifting) of the falling jets as illustrated in Fig. 3. The rapid transition from the bending jet configuration to the mixing configuration shown in Figs. 3(b) and (c) took place in about 1 s. Without further increase in air flow, the system settled into a new equilibrium condition marked by active air–water interaction [Fig. 3(d)].

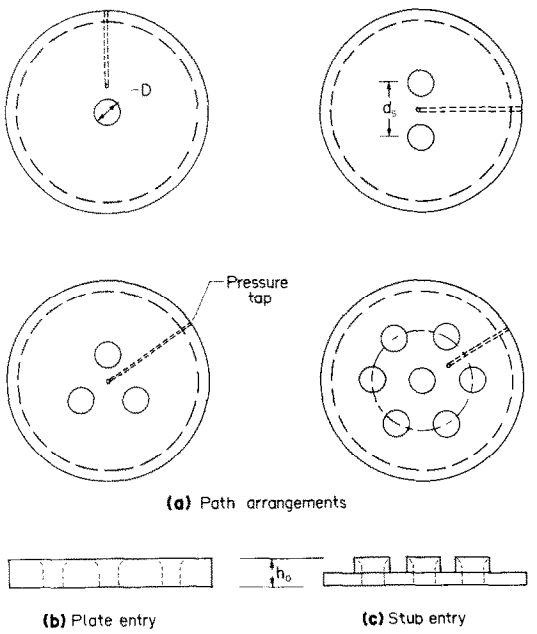

FIG. 2. Typical test section geometries.

A major portion of the experimental results for the onset of flooding as presented in Figs. 4–9 can be bounded by both the Wallis correlation [equation (1) with $m = 0.9$–1.8 and $c_w = 0.5$–1.2] and the Kutateladze correlation [equation (4) with the corresponding c_K and m values shown in the figures]. In terms of the Kutateladze variable, the range of injection rate tested was $0.05 < K_g < 1.10$ for the gas flow and $0.04 < K_l < 0.56$ for the liquid flow. Qualitatively the onset of flooding was promoted by smaller path diameters, a larger number of paths, and smaller path spacing.

A number of tests showed a definite path diameter effect: larger size paths tended to hamper the onset of flooding (Fig. 4). However, the influence appeared to be weak. There were also a few other tests which showed no definite diameter influence. For single-channel flooding, the influence of path diameter is also not fully established [1] but there is some indication that larger size paths may hamper the onset of flooding.

It is evident in Figs. 3(a)–(d) that neighboring paths exerted influence on one another by sending disturbance across the water pool above the test plate. A review of the videotape records suggested that the surface waves generated from the 'early-flooded' paths were responsible, at least partially, for inducing the remaining paths to flood. The experimental results seemed to support the notion that the multiple short-path flow system becomes more susceptible to flooding with increasing number of paths (Fig. 5), but the influence appeared to be weak.

Since the total energy of the surface waves generated from a particular path does not increase, both the amplitude and the density of the disturbance should drop off with the distance as they fan outward across the water pool. This implies that a larger spacing between paths should be less favorable for inducing the onset of flooding. This is clearly shown in Fig. 6, although the effect again appeared to be weak.

It is clear that the medium for surface wave propagation is the water pool above the plate, therefore the amplitude of the disturbance which can propagate across the pool is limited by the pool depth. Then a decrease in the pool depth should effectively reduce the communication among paths by limiting the amount of disturbance transmitted across the pool. This was investigated by replacing the stub entry with the plate entry configuration (Fig. 2), which reduced the pool depth by at least 6.4×10^{-3} m. The experimental results show that plate entry is less favorable for inducing the onset of flooding than stub entry (Fig. 7). In fact it was observed visually that large amplitude waves tended to choke their own propagation by depleting the water layer at some point.

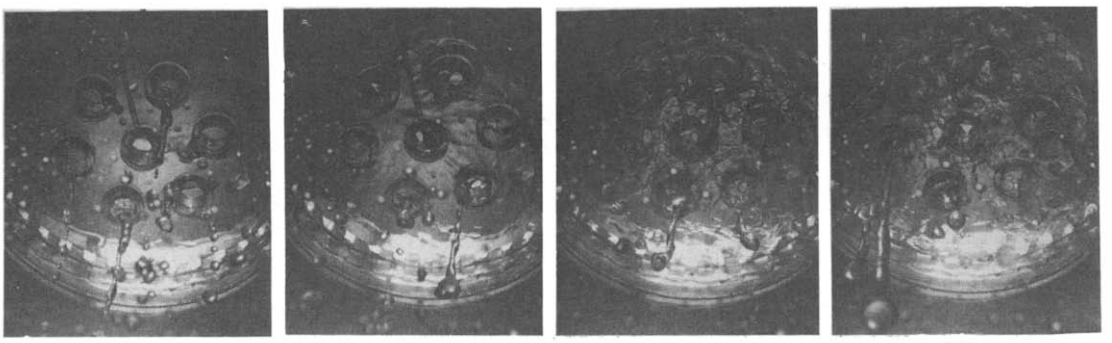

FIG. 3. Sequence of onset of flooding (photographs were taken from below the test plate).

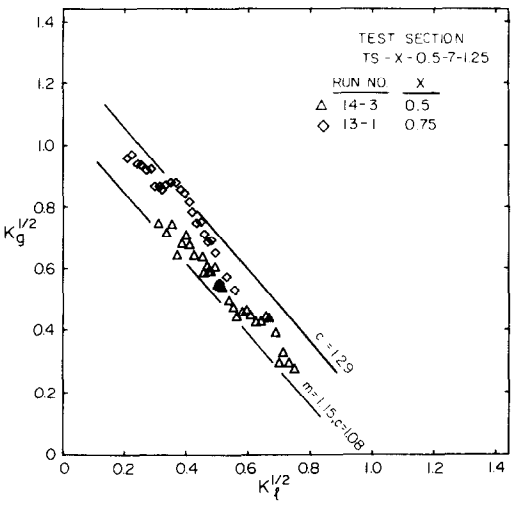

FIG. 4. Path size influence for seven-path configuration.

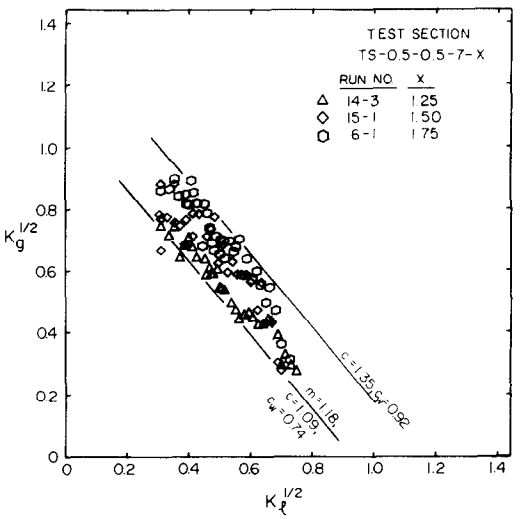

FIG. 6. Effect of path spacing for seven-path configuration with 1.27×10^{-2} m I.D. paths.

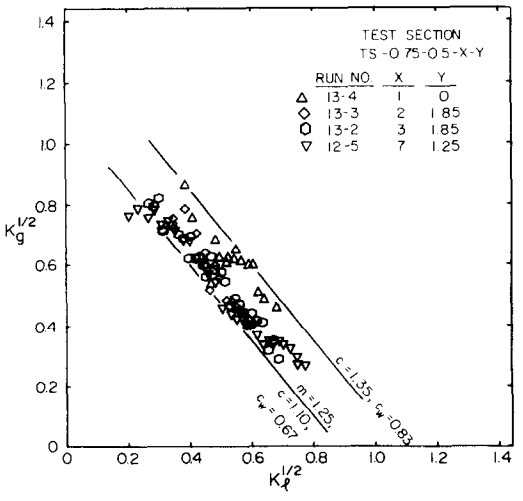

FIG. 5. Influence of number of paths for 1.91×10^{-2} m I.D. path.

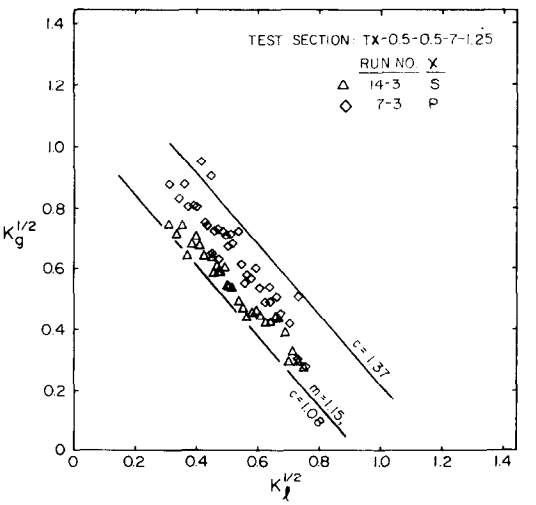

FIG. 7. Plate entry vs stub entry for seven-path configuration.

The various neighboring-path effects discussed above do require that some paths be flooded earlier than the rest. This implies that the initial water distribution among paths is not even, as shown in Fig. 3(a). It can then be speculated that if the initial air–water flow rate is distributed evenly across the test plate, the onset of flooding should be simultaneous across all paths. In this case, the presence of neighboring paths should not make any difference.

Summary of multiple short-path flooding characteristics

If the initial water flow is evenly distributed in each path, and there is no mal-distribution in the subsequent air injection, then the onset of flooding for multiple-path flow will have identical characteristics as that for single-path flow on per-path basis, and the flooding velocities can be bounded either by the Wallis correlation [equation (1)], or by the Kutateladze correlation [equation (4)]. However, with an uneven initial water distribution, the path configuration (i.e. the number of paths and path spacing) exerts secondary influences on the flooding behavior: a larger number of paths and smaller path spacing appear to be a more favorable condition for inducing the onset of flooding. These influences are the consequence of the communication among neighboring paths. Such communication is possible only if there are delays in the onset of flooding in different paths, and such delays are possible only if the initial water distribution is uneven. The communication takes the form of disturbance waves propagating across the water pool on the top of the test plate; the exact amount of disturbance received by a particular path from its neighbors depends on the path configuration and the uneveness in the initial water distribution.

Comparison with previous results

Cervanka and Kolar [7] and Takahashi, Akagi and Kishimoto [8] have investigated the initial accumulation of water on a perforated plate caused by the counterflowing air. The resulting flow rate pairs exhibited the familiar negative slope described by the Wallis and the Kutateladze correlations (Fig. 8). In comparison with the results obtained for TS-0.5-0.5-7-1.25, all three groups of data appear to fall in the proximity of one another. Also included in Fig. 8 are selected experimental results obtained by Bankoff, Tankin and Yuen [9] for air–water CCFL (countercurrent flow limit) through a perforated plate. These CCFL results lie well above the onset of flooding results. Lee and McCarthy [10] studied onset of flooding in multiple short-paths with both low and high liquid buildup above the test plate. These authors also showed that results obtained with large pool depth were substantially higher than those obtained with a small pool depth.

Complete-bypass

A series of flooding tests were performed to investigate the complete-bypass phenomenon. With one

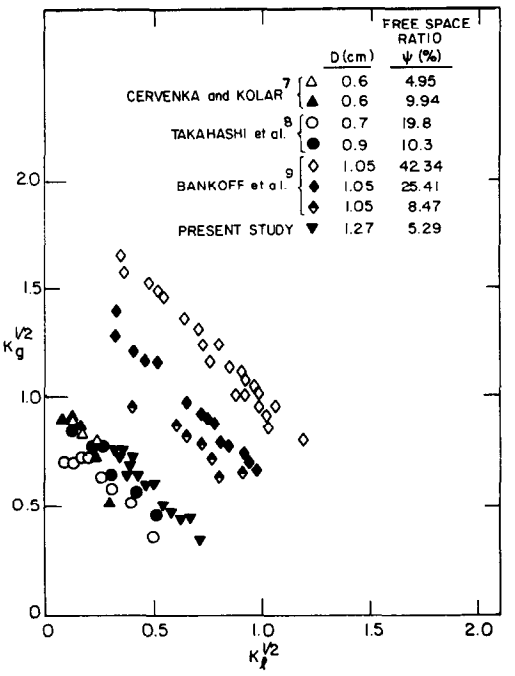

FIG. 8. Comparison with previous results.

1.91×10^{-2} m I.D. overflow situated 0.153 m above the test section TS-1.2-0.5-1-0, the critical K_g for the onset of complete-bypass was found to be around 2.85, independent of the liquid injection rate, and the critical K_g for the end of complete-bypass was around 2.36, also independent of the liquid injection rate.

Pushkina and Sorokin [11] obtained a critical $K_g \sim 3.2$ for zero liquid penetration inside a single glass tube, where the zero penetration criterion corresponded either to the formation of a hanging film or the occurrence of liquid flow reversal inside the tube. The hanging film criterion was also employed by Wallis and Makkenchery [12], and their results varied from $K_g \sim 1.0$ to ~ 3.2 for various tube sizes and materials (glass and Plexiglas) but showed no dependence on the liquid injection rate. It seems reasonable to conclude that the gas flow rate needed to completely stop the liquid penetration is independent of the liquid injection rate.

An interesting feature of the complete-bypass results obtained in this experiment is that the results for the end of bypass were substantially lower than that for the onset: $K_g \sim 2.36$ vs $K_g \sim 2.85$. The criterion for the end of bypass corresponded visually to a 'substantial' liquid repenetration (which was still much less than the liquid injection rate) into the lower plenum. This behavior (the onset values higher than the termination values) was also observed between the onset of flooding and 'de-flooding'.

Flooding hysteresis

The hysteretic behavior between the critical gas flow rate needed to initiate flooding and that at the termination of flooding (where the former values are

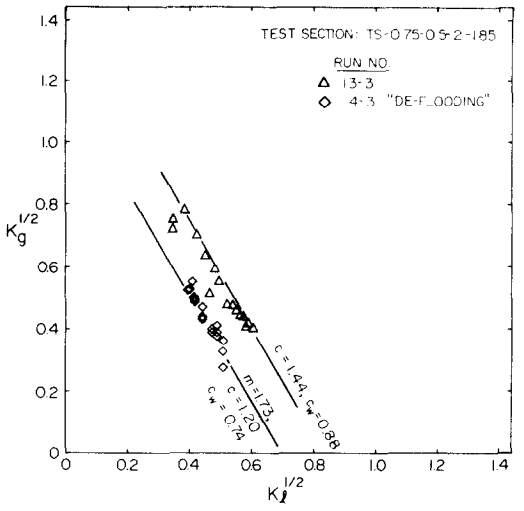

FIG. 9. Flooding and 'de-flooding' hysteresis for two path configuration.

higher than the latter values) is well documented for single-channel flow [1]. In this study, the same hysteretic behavior was also observed in multiple short path geometry (Fig. 9). The criterion for 'de-flooding' adopted here corresponded to the recovery of a continuous water flow through the entire paths by reducing the air injection rate to the point that there was no agitation appearing on the water pool surface above the plate. The resulting 'de-flooding' K_g values are about 35% lower than the onset values.

ANALYTICAL MODELING

Previous models

There have been numerous attempts to derive analytically the Wallis and the Kutateladze correlations as given in equations (1) and (4). Tien, Liu and Chung [1] gave a fairly comprehensive review of the various analyses. Basically, there are two modeling approaches: through instability analysis and through interfacial force balance. Instability analyses on a vertical falling film by Imura, Kusuda and Funtasu [13], Liu, Collier and Cudnik [14], and Tien, Chung and Liu [15] are based on the Kelvin–Helmholtz instability concept originally developed for a stratified heterogeneous fluid with the different layers in relative motion. These authors were primarily interested in predicting the onset of flooding. The interfacial momentum balance approach is favored by Wallis and his co-workers [16, 17], where attention is on the subsequent flooding behavior.

Both approaches have generated correlations similar to equations (1) and (4). A careful examination of these analyses reveals that there are a number of key assumptions associated with each approach, which lead these analyses to their final solution forms. In the instability approach [13–15], the first key assumption is that the perturbed interface boundary condition between the gas and the liquid stream in the vertical direction is given by

$$P'_l - P'_g = -\sigma \frac{\partial^2 \eta}{\partial y^2} \tag{6}$$

where P'_i is the small pressure perturbation, η the interface displacement, and y the coordinate perpendicular to the direction of the bulk flow; and the second key assumption is that the velocity potential, ϕ_i, can be expressed as the sum of the average motion $U_i y$ and the small disturbance ϕ'_i,

$$\phi_l = -U_l y + \phi'_l \quad \text{and} \quad \phi_g = U_g y + \phi'_g \tag{7}$$

where the plus and minus signs account for the directions of the counterflow. The substitution of equation (7) into the Bernoulli equation yields the small pressure perturbation terms

$$\frac{P'_i}{\rho_i} = -\frac{\partial \phi'_i}{\partial t} + U_i \frac{\partial \phi'_i}{\partial y} \quad (i = g, l) \tag{8}$$

where t designates time. One can see that equations (6) and (8) guarantee a solution form of

$$f_1(\rho_g U_g^2) + f_2(\rho_l U_l^2) = \text{constant}. \tag{9}$$

The differences among the various analyses are essentially over the different approximations and simplifications used in each analysis to reduce equations (6) and (8) into a simple form. The ideas of wave growth and interface instability were all once introduced into

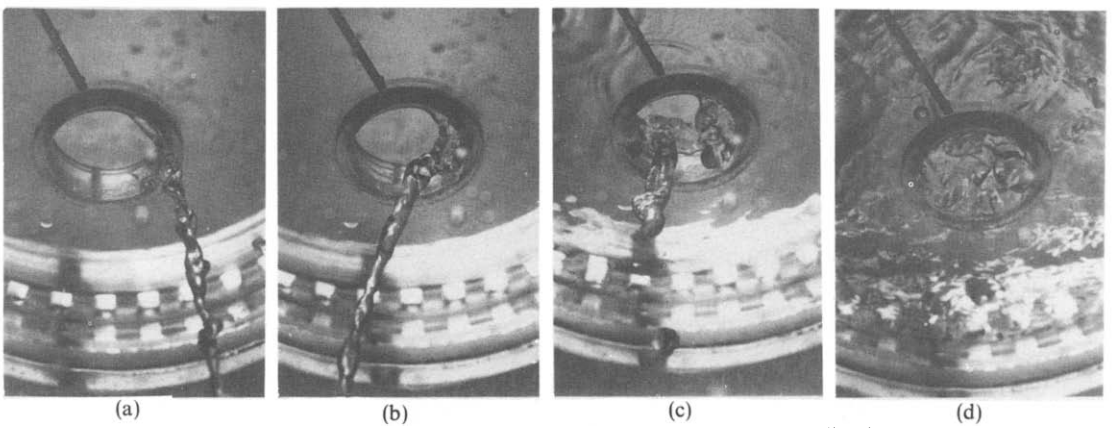

FIG. 10. Sequence of onset of flooding for TS-1.2-0.5-1-0 (single falling-jet).

these analyses; however, they were then removed through the subsequent simplifications, with only the small disturbance assumption preserved in the final solutions.

The key assumption in the interfacial force balance approach [16–18] is the shell balance on the falling film

$$\frac{4\tau_w}{D} + \frac{4\tau_i}{D\alpha^{1/2}} = (\rho_l - \rho_g) g (1 - \alpha) \qquad (10)$$

where τ_w is the wall shear stress, τ_i the interfacial shear stress, and α the void fraction. Since the shear stresses can be written as

$$\tau_w = \frac{1}{2} C_w \rho_l U_l^2 \quad \text{and} \quad \tau_i = \frac{1}{2} C_i \rho_g U_g^2 \qquad (11)$$

where C_w and C_i are the friction factors, then equations (10) and (11) also guarantee a solution form similar to equation (9). Again, the efforts in the various analyses were devoted to the assessment of the parameters in equations (10) and (11).

The common interpretation for equation (1) is that the J_i variable represents a balance between the momentum flux and the buoyant force [1, 19], which is reflected by equation (10); and for equation (4), the interpretation is that the K_i variable represents a balance between the momentum flux and the interfacial surface tension [1, 15], which is reflected by equation (6). However, there is still another interpretation for equations (1) and (4), which treats these correlations themselves as the dynamic similarity conditions describing the occurrence of certain flooding events. This is a consequence of a new modeling procedure developed in this work, which is substantially different from the above mentioned approaches. A detailed discussion of this modeling development can be found in the report by Liu, Tien and McCarthy [6].

A finite amplitude approach

The central idea of this modeling approach is to identify the characteristic physical flow configuration prior to the onset of flooding and to model this flow configuration as closely as possible. An example is given below for flow through a single short path, which illustrates the mechanics of this modeling approach. First to be discussed is the single falling-jet configuration which was observed most often during the experiment. The physical situation is shown in Figs. 10(a)–(d). The onset of flooding corresponded to the instant when the liquid film around the path inlet spilled into the path [Fig. 10(c)]. The characteristic flow appearance can be then identified as the lifting of the triangular web [Fig. 10(b)], and the onset-of-flooding problem is effectively reduced to a 'lifting-web' problem.

In order to lift the triangular web into a near horizontal position, the gas flow must produce enough drag to overcome the downward momentum of the falling web, or

$$\Delta p = C_1 \rho_l U_l^2 \qquad (12)$$

where Δp is the pressure drop across the web, U_l the average liquid velocity at the path exit, and C_1 a proportionality constant. The total pressure drop is estimated to be

$$\Delta p = \frac{3}{4} \rho_g U_g^2. \qquad (13)$$

The average gas velocity U_g in equation (13) is related to the volumetric flow rate Q_g by

$$U_g = \frac{Q_g}{\pi R^2 - A_w}, \qquad (14)$$

where R is the radius of the circular flow path, and A_w is the area blockage caused by the lifting of the triangular web. For a first-order approximation, it is reasonable to assume that the distance between the base and the tip of the web h_w varies with the dynamic head of the exiting liquid film

$$h_w \sim U_l^2/g. \qquad (15)$$

The base length of the web L can be obtained from

$$Q_l = U_l \delta L \qquad (16)$$

where Q_l is the volumetric liquid injection rate and δ is the film thickness. The web area A_w can now be written as

$$A_w = \frac{1}{2} L h_w = \frac{C_2}{2} \frac{U_l Q_l}{g\delta} \qquad (17)$$

where C_2 is a proportionality constant. It can be easily shown that equations (12), (14) and (17) yield the desired solution form

$$f_1(Q_g) + f_2(Q_l) = \text{constant}. \qquad (18)$$

A rough estimate of the parametric dependence of U_l on the independent variables (which are Q_g, Q_l, ρ_g, ρ_l, σ, μ and R) can be obtained from the result for a steady falling film flow

$$U_l \sim \frac{\rho_l g \delta^2}{3\mu}. \qquad (19)$$

The film thickness δ can be estimated by applying the minimum energy principle; McCarthy and Lee [20] showed the following relation for δ_{min}:

$$\delta_{min} \sim \left(\frac{15\,\mu^2 \sigma}{\rho_l^3 g^2} \right)^{1/5}. \qquad (20)$$

Equations (19) and (20) imply that h_w (the web height) is independent of Q_l. However, high speed photographs showed that this was not the case, rather both h_w and L (the web base length) grew as Q_l increased. But as an approximation, the above two equations seem to give a reasonable functional dependence for U_l. Then the 'lift' relation [equation (12)] can be

expressed in terms of the independent variables as

$$\frac{3}{4}\rho_g\left(\frac{Q_g}{\pi R^2 - C_4(0.286)(\rho_l^2\sigma/\mu^3 g^2)^{1.5} Q_l}\right)^2 = C_5(0.97)\rho_l\left[\frac{\sigma^2 g}{\rho_l\mu}\right]^{2.5} \quad (21)$$

where C_4 and C_5 are proportionality constants. Equation (21) can be simplified and nondimensionalized into

$$K_g' + (0.325)C_4C_5^{1.2}Im^4K_l' = (1.137)C_5^{1.2}Im \quad (22)$$

where

$$K_i' = \frac{\rho_i^{1.2}j_i}{(\sigma g\rho_l)^{1.4}}; \quad Im = \left(\frac{\rho_l\sigma^3}{\mu^4 g}\right)^{1.20}. \quad (23)$$

The variable K_i' is of the same form as the Kutateladze variable K_i defined in equation (5) except for the density term in the denominator. In actual calculations at atmospheric pressure, the use of ρ_l or $\Delta\rho\,(=\rho_l-\rho_g)$ makes very little difference because of the small values associated with ρ_g (typically 0.1% of ρ_l).

For water the nondimensional group Im has a value around 3.4; equation (22) then reduces to

$$K_g' + (43.42)C_4C_5^{1.2}K_l' = (3.866)C_5^{1.2}. \quad (24)$$

The actual test results as shown in Fig. 11 can be correlated by

$$K_g + 2.38K_l = 0.81, \quad (25)$$

which implies that $C_4 \simeq 0.26$ and $C_5 \simeq 0.04$. Although the values for the constants appear to be low, they seem to be reasonable in light of the number of approximations involved.

When the path is completely wetted ($Q_l \gtrsim 2.49 \times 10^{-5}$ m^3 s^{-1}), the exiting film takes a slightly different contraction form: rather than forming a single contraction zone, there are a number of such contraction zones [therefore the term 'multiple' falling-jets, Fig. 12(a)–(d)].

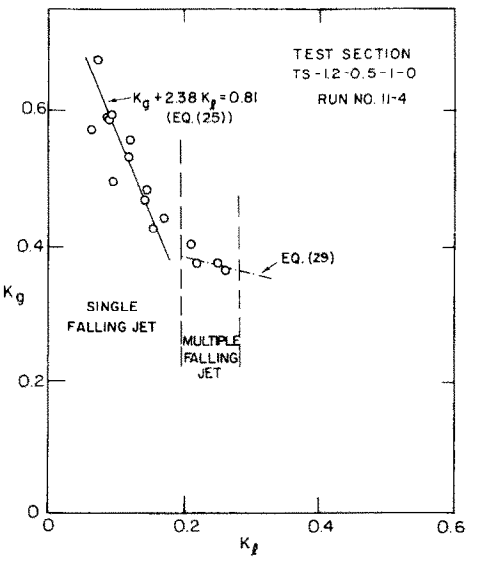

FIG. 11. Experimental results for the onset of flooding for TS-0.2-0.5-1-0.

The extension of the previous analysis to the problem here is fairly straightforward. The mechanism for lifting the webs is the same as before, therefore equation (12) is still applicable. Since all webs are contracted from the same exiting falling film, U_l is assumed not to vary much from web to web. However, when the film wets the entire path wall and forms an annular ring, the film thickness can be expressed approximately as

$$\delta \sim \left(\frac{3\mu Q_l}{2\pi R\rho_l g}\right)^{1/3}, \quad (26)$$

which is just the result for a steady 2-dim. laminar falling film. The associated film velocity is

$$U_l \sim \left(\frac{\rho_l g}{6\mu}\right)^{1/3}\left(\frac{Q_l}{\pi R}\right)^{2/3}. \quad (27)$$

Then the 'lift' relation becomes

$$\rho_g^{1.2}Q_g + \frac{C_6}{6}\left(\frac{4}{3}C_7\right)^{1.2}\frac{\rho_l^{3.2}}{\pi R\mu}Q_l^2 = \left(\frac{4}{3}C_7\right)^{1.2}\frac{\rho_l^{5.6}}{(\pi R)^{2.3}}\left(\frac{g}{6\mu}\right)^{1/3}Q_l^{2.3}(\pi R^2) \quad (28)$$

where C_6 and C_7 are proportionality constants. For an air–water system with a path diameter of 3.048×10^{-2} m (1.2 in), equation (28) can be further simplified into

$$(1.095)Q_g + C_6C_7^{1.2}(1.271 \times 10^8)Q_l^2 = C_7^{1.2}(2.38)Q_l^{2.3}. \quad (29)$$

The four data points obtained in the multiple falling-jet flow region ($2.49 \times 10^{-5} \lesssim Q_l \lesssim 3.40 \times 10^{-5}$ m^3 s^{-1}, Fig. 11) can be correlated with equation (29) by letting $C_6 \approx 7.8 \times 10^{-3}$ and $C_7 = 1$.

For liquid injection rates exceeding 3.40×10^{-5} m^3 s^{-1}, the exiting film no longer breaks up to form falling-jets, rather it contracts directly into a large single falling-jet similar to that shown in Fig. 12(c). Because of the difficulties in finding a distinct visual criterion in the actual testing, no serious attempts were made to obtain any useful results.

There are several consequences brought about by equations (22) and (28). The most important ones are perhaps the concepts of 'lift' and flow area reduction, which were used successfully in deriving an expression for the onset of flooding. Another important point is that the onset of flooding seems to be position preferential, occurring at the location of the largest gas pressure drop—a direct consequence of the 'lift' concept. The initial liquid flow configuration also has a considerable influence on the onset of flooding, which is evident through equations (22) and (28). However, the analysis here is plainly approximate with many key relationships not precisely known. Also, for different geometries, the basic mechanism for inducing flooding may be quite different. Notably, the concept

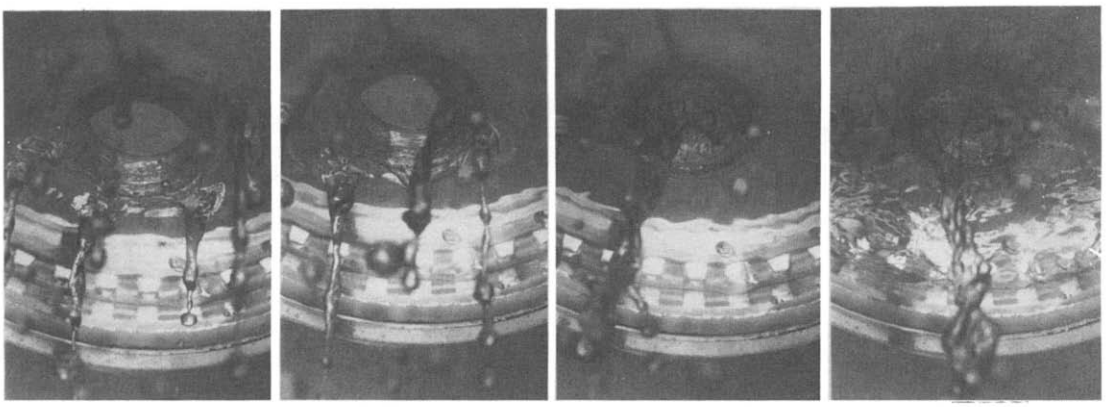

FIG. 12. Sequence of onset of flooding for TS-1.2-0.5-1-0 (multiple falling-jet).

of wave growth remains to be an attractive alternative mechanism for inducing flooding. In fact, based on the wave concept, the presence of flow area contraction or expansion can be interpreted as a strong source of disturbance, which promotes wave growth. For flooding inside flow equipment with no area change, the wave concept may even explain the phenomenon better than the 'lift' concept which requires an area change.

Gas-liquid flooding through multiple short paths

With some of the basic flooding characteristics established for single short-path geometries, the analysis of the flooding behavior through multiple short paths can now be attempted. In the same line of thinking as in the previous section, the condition for the onset of flooding is again

$$\Delta p_n = C_1 \rho_l U_{ln}^2, \quad n = 1, 2, \ldots N \tag{30}$$

where the subscript n denotes the nth path. There is an additional requirement which the gas flow has to satisfy

$$\Delta p_1 = \Delta p_2 = \ldots = \Delta p_N = \Delta p \tag{31}$$

i.e. the pressure drop across each path has to be the same, provided that the paths are not clustered together. This condition is automatically satisfied if equation (21) is assumed to apply (i.e. for partially wetted wall, the liquid momentum is independent of path diameter and flow rate Q_l)

$$\frac{\rho_g^{1/2} Q_{gn}}{\pi R^2 - C_8 Q_{ln}} = C_9 = \Delta p^{1/2}. \tag{32}$$

where C_8 and C_9 are constants. The total gas injection rate is simply the sum of the individual Q_{gn}

$$\rho_g^{1/2} Q_g + C_8 C_9 Q_l = C_9 N \pi R^2, \tag{33}$$

where

$$Q_g = \sum_{n=1}^{N} Q_{gn} \quad \text{and} \quad Q_l = \sum_{n=1}^{N} Q_{ln}. \tag{34}$$

The approximate analysis above suggests that flooding in multiple short paths is similar in nature to that in a single short path, which is in agreement with the experimental results. The characteristics are preserved through the 'additive' nature of the analysis.

The onset of flooding in a single channel

Single channel is a more commonly used geometry in countercurrent flow study. First to be discussed is the partially wetted wall case; the physical situation is shown in Figs. 13(a)–(e). The onset of flooding corresponded to the instance when the falling jet was completely broken up as indicated in Fig. 13(d). The characteristic flow pattern prior to the onset of flooding is again lifting of the falling jet, where the 'lift' relation is still given by equation (12). However, there was no appreciable gas flow area reduction observed during the jet-lifting, therefore the average gas velocity U_g is just

$$U_g = \frac{Q_g}{\pi R^2}. \tag{35}$$

Since the channel surface is partially wetted, the film velocity U_l estimated for the partially-wetted short path as given in equations (19) and (20) is assumed to be applicable here as a first approximation for the falling-jet velocity at the channel exit. Then the 'lift' relation becomes

$$\rho_g j_g^2 = C_{10} \rho_l U_l^2 = C_{10} \rho_l (0.985)^2 \left[\frac{\sigma^2 g}{\rho_l \mu}\right]^{2/5}, \tag{36}$$

which is independent of the liquid injection rate. For air–water systems, equation (36) reduces to

$$K_g = \frac{\rho_g^{1/2} j_g}{(\sigma g \Delta \rho)^{1/4}} = C_{10}^{1/2} (3.337). \tag{37}$$

The actual test results scattered around a mean K_g value of ~ 1.08 (Fig. 14, partially wetted zone) which implies that $C_{10} \sim 0.11$. However, this C_{10} value implies that the falling jet is not completely lifted, which is contradictory to the photographic evidence.

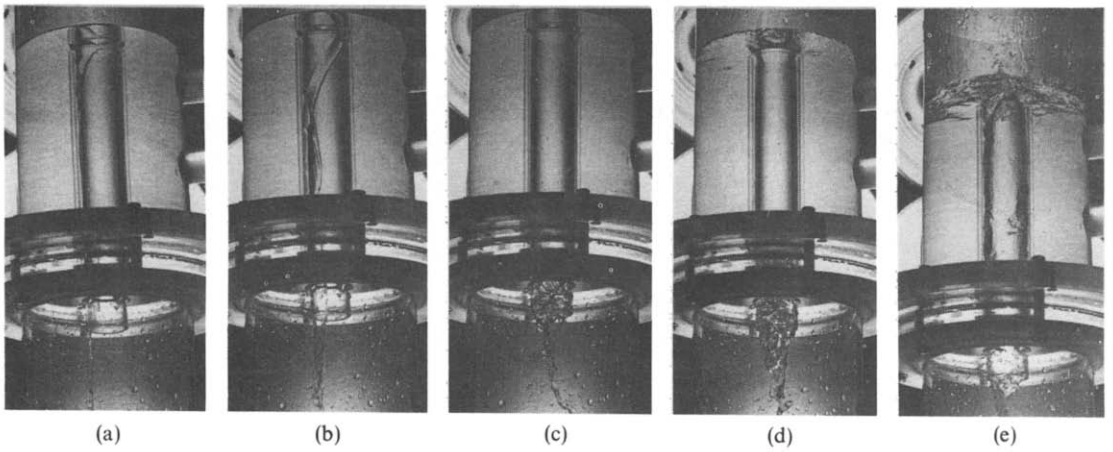

FIG. 13. Sequence of onset of flooding for TS-1.2-10-1-0 (partially wetted-wall).

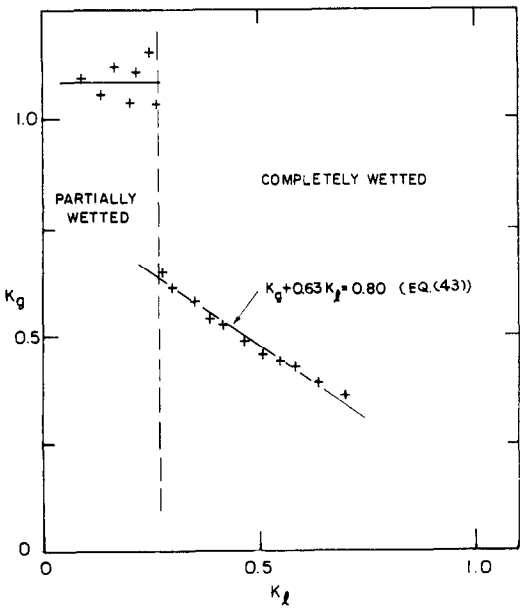

FIG. 14. Experimental results for TS-1.2-10-1-0.

This large discrepancy probably came from the estimate of U_1, which cannot be made accurately without more detailed information.

The onset of flooding for the completely wetted channel wall case ($Q_1 > 3.32 \times 10^{-5}$ m^3 s^{-1}) is depicted in Figs. 15(a)–(f). The onset point corresponded to the instance when the liquid film around the channel inlet spilled into the channel [Fig. 15(e)]. This visual criterion is equivalent to the condition of lifting the gas–liquid mixture from the channel exit, where it is first formed, up to the channel inlet [Figs. 15(c) and (d)]. The momentum transfer between the gas flow and the liquid mass in the mixture is just

$$\Delta M_1 \approx \Delta M_g \tag{38}$$

where ΔM_1 is the change in liquid momentum and ΔM_g is the change in gas momentum during lifting. The distance H which the liquid mass can ascend is approximately proportional to its initial velocity gained from 'lift', or

$$H \approx U_i^2/g \tag{39}$$

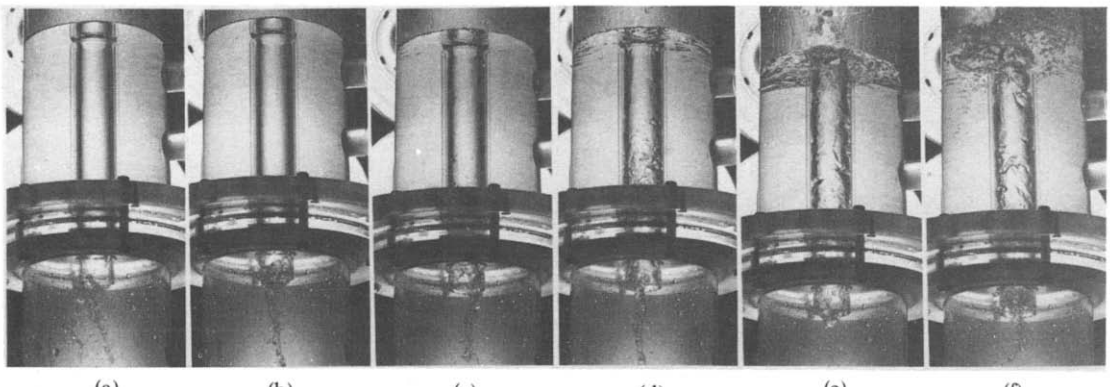

FIG. 15. Sequence of onset of flooding for TS-1.2-10-1-0 (completely wetted-wall).

and

$$\Delta M_l = \rho_l A_l l (U_l + U_i)^2 \quad (40)$$

where U_l is the initial film velocity [given by equation (27)], l is the length and A_l is the frontal area of the liquid mass. The frontal area A_l should have a functional form of

$$A_l \sim A_l(Q_l^x) \quad (41)$$

where x is some unknown exponent. The 'lift' relation then takes on the form

$$\rho_g^{1/2} Q_g + C_{11}[\pi R^2 + A_l(Q_l^x)][Q_l/(\pi R)]^{2/3} + C_{12} H^{1/2} A_l(Q_l^x) = C_{13} H^{1/2} \pi R^2 \quad (42)$$

where C_{11}, C_{12} and C_{13} are constants. The actual test results can be correlated as shown in Fig. 14 by

$$K_g + 0.63 K_l = 0.80. \quad (43)$$

Three concepts have been used extensively throughout the discussion thus far: gas flow area reduction, gas flow contraction, and sequential flooding process. A fourth concept, especially for the channel geometry, is the localized flooding behavior. The use of 'localized flooding' simply means that the most intense countercurrent mixing occurs at specific locations, and the flow elsewhere in the system is governed by the motions at these locations. This is a consequence of the onset of flooding being position preferential. Localized flooding is clearly evident in the series of photographs shown in Figs. 13 and 15. With the inclusion of the inlet and exit regions of a channel, which are normally not shown in photographs depicting flooding, it became obvious that the so-called chaotic appearance inside the channel, often cited as a criterion for flooding, is caused either by the disintegrating mixture originating from the channel exit [Fig. 15(d)] or by the unsteady issuing of liquid at the path inlet resulting from the mixing action at that location [Fig. 15(f)].

Dynamic similarity

A major portion of the research efforts in countercurrent two-phase flow is to identify a set of scaling variables such that the test results may be extrapolated to scale-up cases. The two major contenders for scaling countercurrent flow are the Kutateladze K variable and the Wallis J variable. The common interpretation for the K variable is that it represents a balance between the momentum flux and the interfacial surface tension and the J variable represents a balance between the momentum flux and the buoyant force. This is similar to the Reynolds number in single phase flow,

$$Re = (\rho U \lambda)/\mu, \quad (44)$$

which characterizes the ratio between the inertia and the viscous force. The significance of the Reynolds number is of course that it shows how the dynamic similarity between different flow systems can be preserved. However, it is less obvious how the K variable and the J variable preserve the dynamic similarity in a two-phase flow system since there are two separate scaling variables (one for the gas and one for the liquid) for the same flow system. This confusion may be removed by recalling that the Reynolds number was first arrived at from the study of the transition between laminar and turbulent flow in a tube. In this study, the focus is on the transition from separated to mixing flow (the onset of flooding). The criterion for the onset of flooding is the 'lift' relation [equation (12)] which can be recast into

$$\rho_g U_g^2 = C_1 \rho_l U_l^2 \quad (45)$$

where C_1, the proportionality constant, can be regarded as a characteristic parameter for flooding to be determined experimentally. An analogy can be immediately drawn between the Reynolds number and equation (45): the dynamic similarity condition for the onset of flooding is just equation (45), or

$$C_1 = \frac{\rho_g U_g^2}{\rho_l U_l^2}, \quad (46)$$

which can be interpreted as a ratio between the gas and the liquid momenta. With regard to the Wallis and the Kutateladze correlations, it can be stated that these correlations are themselves dynamic similarity conditions describing the occurrence of certain events in a two-phase countercurrent flow system.

CONCLUSIONS

The above findings may be summarized into three major conclusions:

(1) Flooding in multiple short paths exhibits similar characteristics as that in a single path, with some secondary behavior unique to the multiple short-path flow.

(2) Flooding can be thought of as a consequence of an active gas–liquid interaction, where the momenta in the two flows should be comparable, i.e.

$$\rho_g U_g^2 = C_1 \rho_l U_l^2.$$

(3) The negative slope in the flooding correlations probably comes from the flow area blockage by the resident liquid inside the path, i.e.

$$A \sim A(Q_l).$$

Acknowledgement—This research was supported by the Electric Power Research Institute, Palo Alto, California, through Project 1160-1.

REFERENCES

1. C. L. Tien, C. P. Liu and K. S. Chung, A review of vertical two-phase countercurrent flooding, in *Heat and Mass Transfer in Metallurgical Systems* (edited by D. B. Spalding and N. H. Afgan) pp. 579–596. Hemisphere, Washington (1981).
2. C. P. Liu and C. L. Tien, A review of gas–liquid countercurrent flow through multiple paths, presented at International Seminar on Nuclear Reactor Safety Heat Transfer, Dubrovnik, Yugoslavia (1980).

3. G. B. Wallis, Flooding velocities for air and water in vertical tubes, UKAEA Report AEEW-R123 (1961).
4. C. L. Tien, A simple analytical model for countercurrent flow limiting phenomena with condensation, *Lett. Heat Transfer Mass Transfer* **4**, 231–238 (1977).
5. S. S. Kutateladze, Elements of the hydrodynamics of gas–liquid systems, *Fluid Mech., Soviet Res.* **1**, 29–50 (1972).
6. C. P. Liu, C. L. Tien and G. E. McCarthy, Flooding in vertical gas–liquid countercurrent flow through parallel paths, EPRI-NP-2262 (1982).
7. J. Cervanka and V. Kolar, Hydrodynamics of plate columns. X. Analysis of operation of sieve plates without downcomers, *Coll. Czech. Chem. Commun.* **38**, 3749–3761 (1973).
8. T. Takahashi, Y. Akagi and T. Kishimoto, Gas and liquid velocities at incipient liquid stagnation on a sieve tray, *Int. Chem. Engng* **19**, 113–118 (1979).
9. S. G. Bankoff, R. S. Tankin, M. C. Yuen and C. L. Hsieh, Countercurrent flow of air/water and steam/water through a horizontal perforated plate, *Int. J. Heat Mass Transfer* **24**, 1381–1395 (1981).
10. H. M. Lee and G. E. McCarthy, Liquid carry-over in air–water countercurrent flooding, paper to be presented in the *7th Int. Heat Transfer Conf.*, Munich (September, (1982); EPRI-NP-2344 (1982).
11. O. L. Pushkina and Y. L. Sorokin, Breakdown of liquid film motion in vertical tubes, *Heat Transfer, Soviet Res.* **1**, 56–64 (1969).
12. G. B. Wallis and S. Makkenchery, The hanging film phenomenon in vertical annular two-phase flow, *J. Fluids Engng* **96**, 297–298 (1974).
13. H. Imura, H. Kusuda and S. Funatsu, Flooding velocities in a counter-current annular two-phase flow, *Chem. Engng Sci.* **32**, 78–87 (1977).
14. J. S. K. Liu, R. P. Collier and R. A. Cudnik, Flooding of countercurrent steam–water flow in an annulus, in *Topic in Two-Phase Heat Transfer and Flow*, ASME, New York, pp. 107–113 (1978).
15. C. L. Tien, K. S. Chung and C. P. Liu, Flooding in two-phase counter-current flows—I. analytical modeling, *Physicochem. Hydrodynam.* **1**, 195–207 (1980).
16. G. B. Wallis, H. J. Richter and D. Bhanathan, Air-water countercurrent annular flow in vertical tubes, EPRI-NP-786 (1978).
17. H. J. Richter, Flooding in tubes and annuli, presented at International Seminar on Nuclear Reactor Safety Heat Transfer, Dubrovnik, Yugoslavia (1980).
18. Y. Zvirin, R. B. Duffey and K. H. Sun, On the derivation of a countercurrent flooding theory, ASME Symp. on Fluid Flow and Heat Transfer Over Rod or Tube Bundles, pp. 111 (1979).
19. G. B. Wallis, *One-dimensional Two-phase Flow*, McGraw-Hill, New York (1969).
20. G. E. McCarthy and H. M. Lee, Review of entrainment phenomena and application to vertical two-phase countercurrent flooding, EPRI-NP-1284 (1979).

ENGORGEMENT DANS UN ECOULEMENT VERTICAL GAZ–LIQUIDE A CONTRE-COURANT A TRAVERS DE MULTIPLES PASSAGES COURTS

Résumé—Une étude expérimentale porte sur l'engorgement dans l'écoulement à contre-courant vertical gaz–liquide à travers des parcours brefs et multiples. Les résultats expérimentaux montrent des caractéristiques d'engorgement comme ceux de l'écoulement à un seul parcours, mais il existe des comportements secondaires dûs à l'interaction des parcours. On a développé un modèle pour analyser l'établissement de l'engorgement. L'analyse montre que les formulations du type de Wallis et Kutateladze peuvent être interprétées comme une condition de similarité dynamique pour le phénomène de l'engorgement, bien que la dépendance paramètrique détaillée de cette condition soit compliquée.

ÜBERFLUTUNG IN DER SENKRECHTEN GAS–FLÜSSIGKEITS-GEGENSTRÖMUNG BEI DER MEHRSTUFIGEN KURZWEGDESTILLIATION

Zusammenfassung—Eine experimentelle Untersuchung der Überflutung in der senkrechten Gas–Flüssigkeits-Gegenströmung durch mehrstufige Kurzwegdestillen wurde durchgeführt. Die experimentellen Ergebnisse zeigen ähnliche Überflutungscharakteristiken wie die in den einstufigen Apparaten, aber es treten sekundäre Effekte infolge des Zusammenwirkens der einzelnen Stufen beim mehrstufigen Prozeß auf. Ein Modell-Verfahren wurde entwickelt, um das Einsetzen des Überflutens zu untersuchen. Die Ergebnisse zeigen, daß Korrelationen nach den Vorschlägen von Wallis und Kutateladze als eine dynamische Ähnlichkeitsbedingung für das Überflutungsphänomen betrachtet werden können, obwohl die genaue Abhängigkeit dieser Bedingung von den beeinflussenden Parametern sehr kompliziert ist.

ЯВЛЕНИЕ ЗАХЛЕБЫВАНИЯ ПРИ ВЕРТИКАЛЬНОМ ПРОТИВОТОЧНОМ ТЕЧЕНИИ ГАЗА И ЖИДКОСТИ ЧЕРЕЗ СИСТЕМУ ИЗ МНОЖЕСТВА КОРОТКИХ КАНАЛОВ

Аннотация—Проведено экспериментальное исследование явления захлебывания при вертикальном противоточном течении газа и жидкости через систему из множества коротких каналов. Согласно экспериментальным данным характеристики захлебывания в этой системе аналогичны тем, которые типичны для течения по одному каналу, однако при течении через множество каналов отмечены характерные дополнительные особенности, связанные с взаимодействием потоков. Разработана методика математического моделирования для анализа условий захлебывания. Анализ показывает, что корреляции типа предложенных Уоллисом и Кутателадзе можно рассматривать как условия динамического подобия явления захлебывания, хотя полная параметрическая зависимость этого условия гораздо сложнее.